Accepted Manuscript

Title: Optimization of lipid production in *Chlorella vulgaris* for biodiesel production using flux balance analysis

Authors: Roya Parichehreh, Reza Gheshlaghi, Mahmood Akhavan Mahdavi, Ali Elkamel

PII: S1369-703X(18)30376-0
DOI: https://doi.org/10.1016/j.bej.2018.10.011
Reference: BEJ 7062

To appear in: *Biochemical Engineering Journal*

Received date: 21-5-2018
Revised date: 11-10-2018
Accepted date: 12-10-2018

Please cite this article as: Parichehreh R, Gheshlaghi R, Akhavan Mahdavi M, Elkamel A, Optimization of lipid production in *Chlorella vulgaris* for biodiesel production using flux balance analysis, *Biochemical Engineering Journal* (2018), https://doi.org/10.1016/j.bej.2018.10.011

Optimization of lipid production in *Chlorella vulgaris* for biodiesel production using flux balance analysis

Roya Parichehreh[a], Reza Gheshlaghi[a,*], Mahmood Akhavan Mahdavi[a], Ali Elkamel[b,c]

[a] Department of Chemical Engineering, Faculty of Engineering, Ferdowsi University of Mashhad, Azadi Square, Pardis Campus, Mashhad, Khorasan, Iran, Postal Code 9177948944.

[b] Department of Chemical engineering, University of Waterloo, 200 University Avenue West, Waterloo, ON, Canada N2L 3G1.

[c] Department of Chemical Engineering, Khalifa University of Science and Technology, The Petroleum Institute, Abu Dhabi, UAE, PO Box 127788.

[*] Corresponding author: Reza Gheshlaghi, Tel.: (+98) 51 3880 5066; Fax: (+98) 51 3881 6840; E-mail address: gheshlaghi@um.ac.ir.

Roya Parichehreh: Roya_.Parichehreh@mail.um.ac.ir

Reza Gheshlaghi: gheshlaghi@um.ac.ir

Mahmood Akhavan Mahdavi: mahdavi@um.ac.ir

Ali Elkamel: aelkamel@uwaterloo.ca

Highlights

- A fully compartmentalized metabolic model was developed for algal metabolism.
- Flux balance analysis was used to optimize growth and lipid of *Chlorella vulgaris*.
- Growth behavior was predicted at *conditions* without and with nitrogen feeding.
- Physiological pathways of microalgae for lipid biosynthesis were identified.
- CO_2 was the most important limiting factor for lipid under nitrogen starvation.

Abstract

Microalgae, the world's largest group of photosynthetic organisms, convert atmospheric CO_2 to polar and neutral lipids using sunlight, which after esterification can be utilized for biodiesel production. In the present study, a fully compartmentalized metabolic network was developed to describe the metabolism of *Chlorella vulgaris* based on known enzymatic reactions and typical metabolic pathways of green algae. Flux balance analysis was employed to optimize the specific growth rate and the lipid production rate using measured exchange fluxes of the metabolites. The experimental data for batch and fed batch algal fermentation systems acquired from the literature were used to validate the accuracy of the pseudo- steady state model. The physiological pathways of the microalgae for lipid biosynthesis were identified. The simulation revealed that the microalgae would be able to produce higher levels of lipid content (43.6%) during N-starvation cultivation under 100 $\mu mol.m^{-2}.s^{-1}$ light intensity, 0.25 vvm aeration with 2% (v/v) CO_2, 2 $mg.L^{-1}$ PO_4-P, and 5 $mg.L^{-1}$ NO_3-N. Sensitivity analysis showed that CO_2, light energy, O_2, and nitrate were the most important factors affecting the lipid production at N-deficient conditions. The findings consequential for manipulation of the metabolism of the microalgae with optimal activity.

Keywords: Biodiesel, Flux balance analysis, Carbon utilization, Lipid optimization, *Chlorella vulgaris*, Sensitivity analysis.

Nomenclature

CUR	carbon dioxide uptake rate ($mmol.h^{-1}$)
L	logarithmic sensitivity (dimensionless)
LB	lower bound ($mmol.g_{DW}^{-1}.h^{-1}$)
LC	lipid content (%)
LPR	lipid production rate ($mmol.h^{-1}$)
LUR	light uptake rate ($mmol.h^{-1}$)
NUR	nitrate uptake rate ($mmol.h^{-1}$)
OPR	oxygen production rate ($mmol.h^{-1}$)
S	stoichiometric matrix (dimensionless)

$\boldsymbol{S_k^E}$	stoichiometric matrix of known exchange fluxes (dimensionless)
$\boldsymbol{S_u^E}$	stoichiometric matrix of unknown exchange fluxes (dimensionless)
$\boldsymbol{S_u^I}$	stoichiometric matrix of unknown internal fluxes (dimensionless)
$\boldsymbol{UB}$	upper bound ($mmol.g_{DW}^{-1}.h^{-1}$)
$\boldsymbol{V}$	vector of metabolic fluxes ($mmol.g_{DW}^{-1}.h^{-1}$)
$\boldsymbol{V_k^E}$	vector of known exchange fluxes ($mmol.g_{DW}^{-1}.h^{-1}$)
$\boldsymbol{V_u^E}$	vector of unknown exchange fluxes ($mmol.g_{DW}^{-1}.h^{-1}$)
$\boldsymbol{V_u^I}$	vector of unknown internal fluxes ($mmol.g_{DW}^{-1}.h^{-1}$)
$\boldsymbol{Z}$	objective function ($mmol.g_{DW}^{-1}.h^{-1}$)
$\boldsymbol{\lambda_i}$	shadow price (dimensionless)
$\boldsymbol{\mu}$	specific growth rate (h^{-1})
ω_j	weighting element (dimensionless)

1. Introduction

Due to the fossil fuels crisis in the mid 1970s and the emission of atmospheric carbon dioxide on their combustion, using biofuels to replace diminishing oil reserves has become an important topic worldwide. Among different types of biofuels, biodiesel production has recently attracted much attention [1, 2].

Biodiesel is made from oils of biomass and oleaginous plants such as palm, sunflower, and soybean [1]. During recent years, a lot of research reports have described the advantages of using microalgae over other available resources for biodiesel production, such as rapid growth rate, high photosynthetic efficiency and biomass productivity [3-6], relatively high oil content [7], and fatty acid profile similar to typical vegetable oils [1]. Since the low biomass production rate and lipid content of some algae species are the main obstacles for commercial production of biodiesel, maximizing algal biomass and lipid biosynthesis are necessary for bulk production of algal oil. In this regard, several approaches comprising screening of microalgae [8], bioprocess optimization [9], medium optimization [10], genetic manipulation [11], and mathematical modeling [12] have already been used to increase algal biomass and lipid yield.

Metabolic flux analysis (MFA) is a suitable methodology for mathematical modeling of metabolic pathways. Among different flux analysis techniques, flux balance analysis (FBA) has been developed and applied to determine

pseudo steady state metabolic flux distribution in complex biochemical and biological systems in the past three decades. FBA is an optimization-based approach that requires stoichiometric information about the metabolic pathway and relies on relatively strong measurements of extracellular metabolites [13]. FBA has been utilized in a diverse range of applications including metabolic engineering [14], development and analysis of metabolic networks at genome-scale [15], analysis of gene deletion effects [16], identification of drug target [17], as well as in refinement of biochemical/metabolic networks [18].

Due to the increasing interest in microalgae as multi-use feedstocks, some metabolic models have been proposed for better understanding of algal metabolic networks. In simple models, each algal cell was considered as a black box, in which merely production and consumption rates were considered [19, 20]. A relatively simple metabolic model has been developed to describe the primary metabolism of *Chlorella pyrenoidosa* when cultivated under autotrophic, heterotrophic, and mixotrophic conditions. In this model, the effect of light on carbon and energy metabolism was investigated using MFA. The model comprised chloroplast and cytosol compartments, in which all the processes except Calvin cycle were placed in cytosol. Furthermore, the metabolic pathways in biosynthesis of different cellular macromolecules such as carbohydrates, proteins, nucleic acids, chlorophylls and lipids were not investigated [21]. In other proposed models, the construction of two extensive metabolic models elucidating the metabolism of *Chlamydomonas reinhardtii* has been described. These models had a high level of compartmentalization but the localization was not known for a number of reactions and there was limited information regarding the metabolites exchange between the compartments. The quantitative validation of the model was very limited, and only the way algae controls the hydrogen biosynthetic pathways was investigated [22, 23]. A more condensed metabolic model has been developed for the description of the growth and metabolism of *C. reinhardtii*. In the proposed model, only photosynthetic light reactions and Calvin cycle were compartmentalized and transport steps were not accurately considered. The energy parameters for biomass formation and maintenance were determined using the results of chemostat experiments at different growth rates [24]. Another metabolic model was also constructed to explain the phenotypes of *Chlorella* sp. FC2 IITG under photoautotrophic and heterotrophic conditions. Flux distributions were predicted during a transition from nutrient repletion to nutrient starvation phases of the growth using FBA. The model employed the maximization of biomass and neutral lipid as the objective functions during only nutrient deficient-phase [25]. Recently, a genome-scale metabolic model has been proposed to elucidate the metabolism of *Chlorella vulgaris* UTEX 395 (iCZ843) under photoautotrophic, heterotrophic, and mixotrophic growth conditions.

In this model, the aim was to maximize the specific growth rate and the influence of medium compositions (e.g. glucose, acetate, glycerol, and nitrate) on central carbon metabolism and biosynthetic pathways of amino acid, pigment, and nucleotide were studied at different trophic conditions. Although, the model comprised 843 genes, 2,294 reactions, and 1,770 metabolites that were distributed among six compartments (thylakoid, chloroplast, mitochondrion, glyoxysome, cytoplasm, and extracellular space), but its high complexity did not allow direct comparison of the simulation results with the experimental data [26]. Still, more fundamental studies in algal metabolism would be required to understand and predict the ways that algae regulate the lipid biosynthetic pathways in response to different environmental and nutritional perturbations.

In this study, FBA was used as an optimization tool for determination of the intracellular metabolic fluxes and the maximum theoretical specific growth and lipid production rates for oleaginous green microalgae *C. vulgaris*. The aim of this work was to develop a comprehensive metabolic model, simulate the behavior of the photosynthetic organism, predict the effect of cultivation factors on the lipid yield, and identify the metabolites that significantly enhance lipid production using sensitivity analysis concept. To elucidate the practical applicability of the given model, the simulation results of growth and algae metabolic functions were validated with the experimental results inferred from other works in the literature.

2. Materials and methods

Mathematical modeling usually represents a successful approach to analyze the complex biological and biochemical processes [27, 28]. In some biochemical systems, there is insufficient kinetic information about metabolic pathways in the organism under investigation. Therefore, metabolic engineering techniques such as FBA that involves less detailed kinetic information is required [29]. FBA can calculate the fluxes through metabolic pathways using a stoichiometric model and by applying mass balance equations for all metabolites in the network assuming pseudo steady state condition [30, 31]. Thus, FBA provides comprehensive information regarding metabolic networks and their capacity, by which phenotype behavior of the organisms may be predicted in response to variation in environmental and cultural conditions [32].

2.1. Metabolic network construction

The construction of metabolic network that presents the way in which metabolites are interconnected is an important step for analysis of biochemical systems by FBA [27]. In this study, a fully compartmentalized stoichiometric model explaining the primary metabolism of *C. vulgaris* was developed according to different literature [25, 26, 33-37] and the KEGG database [38]. The model contained four cell compartments including chloroplast, mitochondrion, peroxisome, and cytosol. Translocators/shuttles transported the compounds between the different cell compartments. Some of the compound translocators were not known, so the assumptions had to be considered here (e.g. R15.23, R15.24, R15.27, R16.9, R16.14, and R16.19). In the case that the metabolic network information of *C. vulgaris* was either inadequate or completely lacking, the data from *C. pyrenoidosa* [21] and *C. reinhardtii* [22, 39] was included. It is worth to mention that using the metabolic pathways information of closely related microorganisms is very common in metabolic flux analysis approach [24-26]. The resulting network consisted of 347 enzymatic reactions, 195 transport processes, and 258 metabolites. The list of the metabolites and reactions are presented in Appendices A and B, respectively.

Fig. 1 illustrates a general scheme of the metabolic network. According to this figure, light energy absorbed by photosystems stimulates the photosynthetic electron transport, resulting in O_2 release, $NADP^+$ reduction, and ATP synthesis through the light reactions. The stoichiometry of the photosynthetic light reactions is dependent on environmental conditions. In this model, it was assumed that a constant stoichiometry of 8 mol photons yielded 2 mol NADPH, 2.6 mol ATP and 1 mol O_2 [40].

Thereafter, NADPH and ATP produced by the photosynthetic light reactions are consumed for reduction of CO_2 to triosephosphate (TP) via a series of photosynthetic carbon reactions (Calvin cycle) in the stroma. Photosynthetic CO_2 fixation is the first stage in Calvin cycle that is catalyzed by rubisco. This enzyme also exhibits an oxygenase activity, reacting with O_2 instead of CO_2 through a different pathway called photorespiration. Since both carboxylation and oxygenation occur at the same catalytic site of the enzyme, CO_2 and O_2 as alternative substrates for rubisco can compete to react with ribulose-1,5-bisphosphate. However, the photorespiration occurs at low concentrations of carbon dioxide or high concentrations of oxygen in the algal cells [41]. The photorespiratory cycle involves the cooperative interaction among three compartments of chloroplast, mitochondrion, and peroxisome.

TP that is withdrawn from Calvin cycle can be used for starch synthesis and transported to cytosol. The cytosolic TP is then directed to the glycolytic pathway and may be utilized for sucrose formation. Starch and sucrose as the major storage carbohydrates were considered in the chloroplast and cytosol of algal cells.

The energy stored in carbon compounds is released and transiently stored in ATP for cellular use via the respiratory pathways including glycolysis (EMP), pentose phosphate (PP) pathway, and tricarboxylicacid (TCA) cycle coupled to mitochondrial oxidative phosphorylation pathway. In the metabolic network, PP pathway was considered to operate in both chloroplast and cytoplasm at the same time under different cultivation conditions. In mitochondrial oxidative phosphorylation pathway, the amount of ATP generated per oxygen atom reduced (i.e., the P/O ratio) was assumed a fixed value of 2.5 and 1.5 for NADH and $FADH_2$ upon respiration, respectively [42].

The biosynthesis of nucleic acids and proteins are closely linked to the central carbon metabolism. First, glutamine and glutamate are produced by the successive actions of glutamine synthase and glutamate synthase from ammonium generated by photorespiration or nitrate reduction. Thereafter, nitrogen can be transferred from glutamine and glutamate to many carbon backbones such as 3-phosphoglycerate, pyruvate, and oxaloacetate through the transamination reactions to synthesize other amino acids, nucleic acids and proteins. In the metabolic network, the proteins were constituted by summation of the molar fractions of the different amino acids isolated from *C. vulgaris*.

A vast variety of lipids can be produced by higher plants and algae. The lipids play significant physiological roles in plants, such as intercellular signaling, structural support as membranes, and energy storage. Storage lipids mainly contain triacylglycerol (TAG) and can be converted to fatty acid methyl esters (FAME) as biodiesel via transesterification [6, 43].

Lipid biosynthesis from fatty acids is identical in algal and plant cells. Fig. 2 shows a general biosynthetic pathway of TAG in the plant cells based on Kennedy pathway [44]. At the first unique step of the pathway, acetyl-CoA is transduced into malonyl-CoA by adding carbon dioxide in a reaction catalyzed by Acetyl-CoA carboxylase (ACCase) [45]. Then, malonyl-CoA ACP transacylase (MAT) catalyzes the transfer of malonyl-CoA to a protein cofactor, acyl carrier protein (ACP), to generate malonyl-ACP. In the next step of fatty acid synthesis, precursor acyl-ACP chains are lengthened by two-carbon unit per cycle by the action of beta-ketoacyl-ACP synthase (KAS), beta-ketoacyl-ACP reductase (KAR), beta-hydroxyacyl-ACP dehydrase (HAD), and enoyl-ACP reductase (EAR) through subsequent series of condensation, reduction, dehydration, and again reduction reactions, respectively. The

cycle continues until C16:0-ACP and C18:0-ACP are formed. Thereafter, a series of desaturase enzymes act sequentially to make further modification and additional double bonds in some fatty acids for production of C16:3 and C18:3 [46]. Then, acyl-ACP thioesterase (FAT) catalyzes the removal of the acyl group from ACP and generation of palmitic (C16:0) and stearic (C18:0) acids as the final products of fatty acid synthesis. Part of the free fatty acids is transferred to cytosol and the rest is being utilized for TAG biosynthesis. The TAG biosynthesis occurs through successive transfer of fatty acids from Acyl-CoA to GLYC3P via the direct glycerol pathway [47, 48]. Transfer of fatty acid to position one of GLYC3P results in the production of lyso-phosphatidic acid (LPA) in a reaction catalyzed by glycerol-3-phosphate acyl transferase (GPAT). Transfer of the second acyl group to position two of LPA by the action of Lysophosphatidic acid acyltransferase (LPAAT) formed phosphatidicacid (PA). In the penultimate step of TAG biosynthesis, phosphatidic acid phosphatase (PAP) catalyzes PA dephosphorylation, which leads to the production of diacylglycerol (DAG). In the final step of TAG biosynthesis, transfer of the third acyl group to position 3 of DAG is catalyzed by diacylglycerol acyltransferase (DAGAT) for the formation of a neutral triacylglyceride [46, 48]. The composition of fatty acids in TAG extracted from *C. vulgaris* cells, especially for the a-linolenic acid (C18:3) content, may vary under different cultivation conditions [49]. In the proposed model, it was assumed that the synthesis reactions of lipids occurred in the chloroplast and the TAG molecules were directly used for formation of biomass (R14.1) and the remainder accumulated as energy storage (R18.41). The fatty acid composition of lipids was constant under different growth conditions. Accordingly, TAG was modeled in the form of a glycerol molecule linked with three acetyl-ACP tails. Therefore, the acetyl-ACP content of a TAG molecule was determined by triplicating the molar fraction of the various fatty acids present in *C. vulgaris.* Removing the acyl group from ACP and generating the free fatty acids and their transport to cytosol were also neglected [24].

Some nutrients, especially the macronutrient and micronutrient cations, can be assimilated due to production of complexes with organic compounds. In the metabolic network, assimilation of magnesium was considered for the formation of chlorophyll pigments.

In general, the composition of biomass varies with growth rate and cultivation conditions. However, since the composition of biomass even among different microalgae varies slightly, a single reaction for the biomass formation has been used during the time course of the cultivation, in which a constant biomass composition was assumed [24].

2.2. Metabolite balancing and linear programming

To be able to calculate the fluxes through different metabolic pathways, mass balances around each metabolite were written under pseudo steady state condition as following:

$$S \,.\, V = 0 \quad (1)$$

in which S includes the stoichiometric coefficients of the metabolites involved in different reactions of the metabolic network. For the most biochemical systems, the rank of the matrix S is usually less than the number of unknown fluxes and the system is underdetermined. In order to restrict the solution space and decrease the degrees of freedom of the set of algebraic equations, many measurements are needed. If some fluxes in the vector of metabolic fluxes are measured, Eq. 1 can be written as:

$$S_u^I V_u^I + S_u^E V_u^E = - S_k^E V_k^E \quad (2)$$

The unknown fluxes can be determined by applying constraints to some of the fluxes and optimizing an objective. In case of a linear objective function, a linear programming/optimization approach is employed as follows:

$$\text{Objective function:} \quad Max/Min\ Z = \omega_j \,.\, V_j$$

$$\text{Constraints:} \quad S_u^I V_u^I + S_u^E V_u^E = - S_k^E V_k^E \quad (3)$$

$$LB \le V_j \le UB$$

in which ω_j is the weighting element of the corresponding flux of V_j in the objective function of Z. The first set of constraints includes the steady state mass balance equations. If there are some information regarding the values of exchange fluxes, they will be represented by the second set of constraints. Each constraint in the set introduces the upper and lower bounds for the exchange flux of a metabolite, which either enters or exits the system. In order to be consistent with the characteristics of the Simplex algorithm at the linear programming problem, the solution vector, V_u^I and V_u^E would be always non-negative. Hence, irreversible reactions were constrained to one direction and the reversible reactions were broken down to two individual forward and backward reactions. GAMS environment was utilized for linear programming computations.

In the present study, the objective function was either maximization of specific growth rate (i.e., $Max\ Z = V_{R14.1}$) (section 3.1.1), or lipid production rate (i.e., $Max\ Z = V_{R9.33}$) (sections 3.1.2 and 3.1.3). For both cases, the first series of constrains (mass balance equations under pseudo steady state condition) and the second set of constrains (i.e., positivity of fluxes and experimental exchange fluxes) were implemented to limit the solution space based on the metabolic network and the experimental data. The solution provided the maximum value of the objective

function and the unknown metabolic fluxes. The metabolic fluxes were presented in units of mmol.g_{DW}^{-1}.h^{-1} and the normalized biomass flux indicated μ.

2.3. Sensitivity analysis

Sensitivity analysis represents how a biochemical system responds to a permanent perturbation. The perturbation may be a change in an independent variable (e.g. carbon dioxide uptake rate and light supply rate) in the system. The sensitivity can be expressed using the shadow price and the logarithmic sensitivity of the linear programming. The shadow price is introduced as the sensitivity of the objective function *Z*, as a system property, regarding the change in the *i*th flux, as an independent variable, as following [50]:

$$\lambda_i = \partial Z / \partial V_i \quad (4)$$

The logarithmic sensitivity is defined as the ratio of the relative change in the objective function Z to the relative change in the V_i when the objective function is optimized [51, 52] and can be written as:

$$L(Z, V_i) = \frac{\partial Z / Z}{\partial V_i / V_i} = \frac{\partial \operatorname{Ln} Z}{\partial \operatorname{Ln} V_i} = \frac{V_i}{Z}\lambda_i \quad (5)$$

According to Eq. 5, the logarithmic sensitivities are computed by determination of the fluxes, the optimal objective function, and the shadow prices. It is worth to mention that since the absolute value of the fluxes in a metabolic system are of different order of magnitude, the logarithmic sensitivities are preferred for comparison purposes. In the proposed model, the numerical value of each exchange flux of V_i was defined positive for a substrate and negative for a product and by-product. Therefore, the positive shadow price represents that increase in substrate uptake rate and decrease in product excretion rate can improve the optimal solution. Hereby, the analysis of sensitivity can be used to determine the most effective parameters of cultivation in the metabolism and the biomass and product yield.

3. Results and discussions

3.1. Validation of model predictions

The practical applicability of the proposed metabolic model was investigated using experimental data found from other works in the literature.

3.1.1. Maximization of specific growth rate

Mujtaba et al. [53] studied the autotrophic growth of *C. vulgaris* AG10032 in a bubble-column photobioreactor using BG-11 medium at room temperature (stage I). The photobioreactor had a working volume of 1 L (ID, 6.5 cm; height, 37 cm) [54]. The batch experiments were carried out under continuous fluorescence illumination (100 $\mu mol.m^{-2}.s$). Aeration with filtered air was performed at a rate of 0.15 vvm with 4% CO_2. The BG-11 medium was prepared by dissolving following chemicals in deionized water: Na_2CO_3 (20 $mg.L^{-1}$), K_2HPO_4 (58 $mg.L^{-1}$ or 10 $mg.L^{-1}$ PO_4-P), $NaNO_3$ (1500 $mg.L^{-1}$ or 247 $mg.L^{-1}$ NO_3-N), and other components [55]. A typical result of the batch experiments is shown in Fig. 1(a) of their study, in which the concentration profiles of nitrate and biomass during photoautotrophic cultivations without extra nitrogen feeding and with intermittent nitrogen feeding are depicted (stage I).

At this step, the objective function was maximization of the specific growth rate. It is obvious from the experimental observations (without additional N-feeding case) that nitrate was completely consumed and its concentration reached approximately zero (i.e. 2.223 $mg.L^{-1}$) at the end of experiment. The supply rates of phosphate and bicarbonate were considered as the model inputs, because no experimental data were provided for their consumption rates. Since for each metabolite in the model both influx and efflux are considered, the surplus of the metabolite can exit the network. The maximum photochemical quantum yield was set to 0.8 based on a quantum requirement for oxygen release of 10 (rather than 8 based on the photosynthetic light reaction (R1.1)) [24].

To investigate the effect of nitrogen content on production of biomass, the results of modeling for cultivation without and with additional nitrate feeding were compared. In the experiment without N-feeding, the only source of nitrogen was initial nitrogen presented in the BG-11 medium. The cultivation with N-feeding was carried out at conditions similar to the previous case (stage I), while addition of nitrogen was performed repeatedly in order to maintain the nitrogen level of the culture above 130 $mg.L^{-1}$ as NO_3-N (Fig. 1(a) of [53]). Considering the metabolite profiles (Fig. 1(a) of [53]), the cultivation period split into three separate phases and the mean values of the experimental supply rates of light, carbon dioxide, oxygen, and nitrate during each phase were used as the model inputs. Thereafter, the specific growth rates and the lipid contents were computed based on the proposed model for each phase by the use of experimental data, and compared with the experimental results (Table 1). As seen from Table 1, the model predicted the reported specific growth rates of *C. vulgaris* AG10032 on BG-11 during the time course of the experiment with high degrees of accuracy. The predictions for lipid contents were, however, higher than the experimental data. This may be due to the fact that the catabolic reactions (e.g. lipid oxidation reactions)

and the biosynthetic reactions except biomass formation reaction were not considered in our model. Despite the discrepancy in numerical values, the trends of changes in lipid content were similar when the simulation results compared with the experimental data during the different growth phases in both cases of without and with N-feeding.

Furthermore, the unknown metabolic fluxes such as the production rate of various products and the uptake rate of substrates were determined. The uptake rates were calculated from the difference between the influx and efflux values. LUR, CUR, OPR, and NUR during the time course of the experiment are summarized in Table 1. Figures 3(a), 3(b), 3(c) and 3(d) also show the production rate of macromolecular components of biomass including chlorophyll, protein, carbohydrate, and lipid throughout the course of the photoautotrophic cultivation without and with N-feeding (stage I).

During cultivation without additional N-feeding, in phase I ($0 < t < 1$ Day), the NUR was at a maximum of 0.179 $mmol.h^{-1}$, while the CUR, OPR, and LUR were relatively low. The macromolecular components of biomass commenced to increase during this phase (Figs. 3(a) and 3(b)) and small amount of biomass dry weight was produced by the end of this period. Metabolic flux distribution resulted in a specific growth rate of 0.09308 h^{-1} that showed less than 12% relative error when compared to the corresponding measured value (Table 1).

During phase II ($1 < t < 8$ Day), when the culture was in the exponential phase, more light was absorbed by algal cells, thus more carbon dioxide could be fixed and more oxygen produced. The cell density increased due to the high levels of CUR, OPR, and available light energy for growth and reached 1.392 $g.L^{-1}$ at the end of this phase. Additionally, the cells produced higher amounts of chlorophyll, protein, carbohydrate, and lipid in comparison with the other phases and their production rates increased to the maximum values of 0.0008, 0.0446, 0.0684, and 0.0038 $mmol.h^{-1}$, respectively (Figs. 3(a) and 3(b)). The specific growth rate was predicted to be 0.00997 h^{-1} during this phase that was in good agreement with the measured value of 0.00931 h^{-1}.

In the last phase of the cultivation ($8 < t < 10$ Day), nitrate was completely consumed and the reduced amount of the absorbed light energy decreased the values of CUR and OPR. This led to the slow growth during this phase of the cultivation (1.411 $g.L^{-1}$ biomass density). As nitrogen deficiency was developed, the production rates of chlorophyll and protein in the cells decreased significantly throughout this period, while the lipid and carbohydrate were produced at relatively high rates of 0.0036 and 0.0377 $mmol.h^{-1}$, respectively. The predicted specific growth rate by the metabolic flux model was 0.00029 h^{-1} with the relative error of 7.41%.

The metabolic flux model estimated that the maximum relative error for specific growth rates was 13.67% during the autotrophic cultivation with repeated nitrogen feeding. The same trends were observed for the metabolites uptake rates and the products production rates during the autotrophic cultivation in both cases of without and with N-feeding. Due to the increase in available light energy for growth, CUR, and NUR at cultivation with nitrogen feeding, the production rate of chlorophyll increased compared with the case without N-feeding and the products of photosynthesis were switched from carbohydrate and lipid to protein (Table 1; Fig. 3). Moreover, nitrogen sufficient condition resulted in 45% increase in the final biomass concentration (data not shown). Hence, these results revealed that the presence of nitrate increased the growth rate, while the accumulation of lipid and carbohydrate were decreased, which were in agreement with the reports of the other authors [10, 56]. According to the results, it could be concluded that the growth behavior of the microalgae could be accurately predicted by the proposed model at different cultivation conditions.

Metabolic flux distribution indicated that EMP pathway, PP pathway, TCA cycle, and mitochondrial oxidative phosphorylation remained active during illumination. Only PP pathway located in cytosol was active to provide pentose phosphate for synthesis of nucleic acid in the network of autotrophic metabolism. Since different phases of cultivation were performed at high levels of CO_2/O_2 ratio, the oxygenase reaction rate approached zero and the photorespiration pathway was minimal in the metabolic network. At TAG biosynthesis pathways, the cytosolic pyruvate was used as the main precursor for the plastid acetyl-CoA pool in microalgae under maximal specific growth rate.

3.1.2. Maximization of lipid production

Model accuracy and reliability of its predictions was also examined by comparing the measured lipid contents with the predicted values. Maximization of lipid production rate was employed as the objective function for a certain specific growth rate at the same cultivation conditions with the previous cases (stage I).

Simulation results of cultivations without N-feeding and with repeated N-feeding are presented in Table 2 and compared with the experimental results evaluated from experimental data for each phase (Fig. 1 of [53]). In general, the results showed that the experimental lipid contents were much less than the model predictions, because the cells did not utilize their full biological capacity for lipid production. Nevertheless, the simulation results could still be useful if considered as the highest capacity of the cells for lipid production with a desired fatty acid profile for production of biodiesel. On the other side, the lipid contents presented in Tables 1 and 2 showed that the simulation

results when the objective was maximization of specific growth rate were closer to the experimental data compared with the simulation results from maximization of lipid production rate.

As mentioned in section 3.1.1, in the first phase of the cultivation, the predicted lipid contents were low. Then, the cells produced the lipid at the maximum rate for accumulation and cellular growth within the exponential growth phase. Finally, accumulation of large amount of lipid during the last growth phase increased the lipid content by the end of this phase. Comparisons between the data presented in Table 2 indicated that depletion of nitrogen redirected the flow of fixed carbon to lipid synthesis from protein synthesis and the microalgal lipid content increased during the second (1-8 day) and the third (8-10 day) phases of the cultivation approximately 18% and 19%, respectively. Metabolic flux distribution also revealed that acetyl-CoA as a precursor for synthesis of fatty acids was produced by the cytosolic citrate during the autotrophic cultivation of *C. vulgaris* (stage I) under optimum lipid production condition.

3.1.3. Effects of nutrient availability and environmental factors on lipid production

The validity of the proposed model was also investigated by studying the physiological behavior of the microalgae in response to certain changes in cultivation conditions. The effects of aeration rate, light intensity, and carbon source were scrutinized on total lipid content under selected cultivation conditions. When a desirable cell density was obtained at the first stage, the cells were cultivated under certain conditions (stage II) in nitrogen-deficient BG-11 medium at 25 $^{\circ}$C. At the beginning of stage II, the cell density and lipid content were 1.5 g.L^{-1} and 20% of dried cell weight (DCW), respectively. In the culture, no CO_2 was supplied, except for the case in which the effect of carbon source in the BG-11 medium was to be examined [53].

At this step, the objective function was maximization of the lipid production rate. Due to very low biomass production rate during the stage II, the specific growth rate was assumed to be zero. The simulation results of lipid contents under different cultivation conditions (stage II) are summarized in Table 3 and compared with the experimental results evaluated from experimental data (Figs. 2, 3, and 6 of [53]).

The effect of aeration rate - Different aeration rates varying from 0.125 to 0.5 vvm were used for the possible improvement of lipid content under nitrogen deficient cultivation in a dark environment (stage II). Maximum lipid content was obtained after 12 h in all air flow rates (Fig. 2 of [53]). Therefore, the lipid contents were evaluated by

the model during the same period of time (12 h after incubation) at different aeration rates and compared with the experimental results (Table 3).

Although the experimental lipid contents of the microalgae were quantitatively different from the predicted values, the same trends were observed. As shown in Table 3, the lipid content increased from 27.2% to 34.1% of DCW, when the culture aeration rate was increased from 0.125 to 0.25 vvm. Metabolic flux distribution indicated that higher air flow rates leaded to increase in oxygen transport from cytosol to chloroplast. Hence, chloroplast oxygen and acetyl-CoA produced by cytosolic citrate have been utilized for higher unsaturated fatty acids production at TAG biosynthesis pathways (Fig. 4(a)). According to simulation results, the lipid content decreased with increasing air flow rate to 0.5 vvm and reaching nearly 29.5% of DCW during this period. This was due to the variation in fatty acids biosynthesis pathways and the production of acetyl-CoA from chloroplast pyruvate via the action of chloroplastidial pyruvate dehydrogenase (PDH). On the other hand, part of the oxygen presented in cytosol was consumed by the cytosolic reactions and only a small fraction of oxygen was transported to chloroplast leading to the synthesis of unsaturated fatty acids and lipids (Fig. 4(b)). These results demonstrated that a moderate range of aeration benefits significantly lipid accumulation at N-deficient condition.

The effect of light intensity - The variation of the lipid content profiles during nitrogen depleted cultivation (stage II) with 0.25 vvm aeration and 10 $mg.L^{-1}$ initial PO_4-P under different light intensities indicated the effect of light intensity on the lipid content (Fig. 3 of [53]). After 12 h of cultivation, the maximal lipid content was achieved in the cultures illuminated under different light intensities. The predicted and experimental results of cultivations at different light intensities at 12 h after incubation are presented in Table 3.

The lipid content increased as the light intensity increased and 35.1% of lipid content was obtained in the culture irradiated with 100 $\mu mol.m^{-2}.s^{-1}$ light intensity. Higher levels of absorbed light energy resulted in the increase of O_2 release and the synthesis of ATP and NADPH through the light reactions of photosynthesis in the chloroplast. Due to increase of these photosynthetic products, fatty acids synthesis was increased and higher amount of lipids were produced, ultimately (Fig. 5). Based on the experimental results, higher light supply rates than 100 $\mu mol.m^{-2}.s^{-1}$ showed a minor negative influence on the lipid content but there was no reaction to implement inhibitory effects of light in the model, so the predicted lipid content by the model did not agree with the measured lipid content in the culture irradiated with 200 $\mu mol.m^{-2}.s^{-1}$ light intensity and showed 0.4% increase in the lipid content.

The effect of CO_2 supply - Different CO_2 concentrations in the range of 0–10% was supplied for the possible enhancement of lipid production at the incubation conditions with 0.25 vvm aeration, 100 $\mu mol.m^{-2}.s^{-1}$ light intensity, 2 $mg.L^{-1}$ PO_4-P, and 5 $mg.L^{-1}$ NO_3-N (Fig. 6 of [53]). The experimental results showed that maximum values of lipid contents were obtained at 24 h. The lipid contents were estimated by the model at different CO_2 concentrations at 24 h after incubation and compared with the experimental results (Table 3).

The effect of CO_2 concentration on lipid content was qualitatively identical in experimental and simulated results. The simulation results predicted that the lipid content was increased by adding 2% CO_2 into the cultures of *C. vulgaris* (43.6% DCW). Metabolic flux distribution revealed that the increase of CO_2 supply led to transportation of CO_2 from cytosol to mitochondrion and higher production of mitochondrial isocitrate as a precursor for acetyl-CoA synthesis (Fig. 6(a)). But increasing CO_2 concentration to higher level of 10% had a negative impact on the lipid content. This observation was due to the increase in conversion of CO_2 to bicarbonate in cytoplasm and decrease in concentration of mitochondrial CO_2 in high-CO_2 cells (Fig. 6(b)). Considering all these observations, it could be concluded that higher levels of the key metabolites would not necessarily increase the lipid production rate during the cultivation of *C. vulgaris* and would inhibit the microalgal lipid production.

3.2. Sensitivity analysis

The shadow price and the logarithmic sensitivity values for maximization of lipid production rate were determined at different phases of the cultivation for various metabolites. Since it was not possible to present all the shadow prices and the corresponding logarithmic sensitivities, only a summary of the most significant values for the extracellular metabolites during different phases of the autotrophic cultivation without N-feeding (stage I) are represented in Table 4.

At phase I ($0 < t < 1$ Day), logarithmic sensitivities for all measured metabolites were very small (less than 0.001), except for phosphate, proline, and phenylalanine. For instance, the logarithmic sensitivity value for phosphate was 0.004 during the early phase of the cultivation. Quantitatively, this value meant that 10% increment in the uptake rate of this metabolite would result in 0.04% increment in the lipid production rate during this phase.

In phases II ($1 < t < 8$ Day) and III ($8 < t < 10$ Day), the highest logarithmic sensitivities of 39.711 and 57.731 were observed, respectively for carbon dioxide, indicating carbon dioxide uptake rate was the most important limiting factor for the lipid production during these phases. Moreover, moderate logarithmic sensitivities of 2.549 and 4.866

were observed for oxygen during the second and the third phases, respectively. Since the shadow prices of oxygen were negative, any increase in its production rate would improve the optimal lipid production rate. The absolute values of logarithmic sensitivities of CO_2 and O_2 were significantly higher at phase III compared to phase II. Consequently, higher uptake rate of CO_2 and higher production rate of O_2 would further enhance the objective function at stationary phase. Although, light energy had a moderate shadow price of 0.024 during the second phase of the cultivation, its relatively high uptake rate value resulted in a large logarithmic sensitivity of 26.844, which was high enough to significantly affect the objective function at this period.

The sensitivity analysis also suggested that logarithmic sensitivities of phosphate were very small (approximately 0.011 and 0.023) during these phases, so any change in its uptake flux would not dramatically influence the lipid production rate. Considering these results, one could conclude that the cells might consume phosphate for production of the other products during these periods.

Based on the analysis results, despite high shadow prices of ammonium, this nitrogen source had trivial logarithmic sensitivities. In contrast, the logarithmic sensitivities of nitrate were 1.019 and 3.87 during phases II and III of the cultivation, respectively. Therefore, the lipid production rate was probably affected by the uptake rate of nitrate, especially when the cells were at the final phase of the growth.

Although glycerol as an important factor for glycerol-3-phosphate production in the TAG biosynthetic pathway had the highest shadow prices among the measured metabolites at all phases but its logarithmic sensitivities were very small due to its low uptake rates. Accordingly, glycerol cannot be used to enhance the lipid production at low levels of uptake rate.

Among the biomass components, chlorophyll and DNA had shadow prices of zero at different culture phases, so the lipid production rate was not sensitive to changes in the exchange flux of these metabolites. Besides, sucrose, RNA, and protein had nonzero shadow prices during the second phase and the logarithmic sensitivities of approximately zero (less than 0.001) at all phases of cultivation. In addition, the performed sensitivity analysis showed that all amino acids had the logarithmic sensitivities of zero during these periods of the cultivation. Thus, it can be concluded that the optimal solution was insensitive to any change in exchange fluxes of biomass components and amino acids.

Ultimately the sensitivity analysis revealed that CO_2, O_2, light energy, and nitrate had significant effects on the algal lipid biosynthesis during the autotrophic cultivation under N-starvation. The experimental observations in the

previously published articles were in great agreement with the above mentioned simulation results that the uptake rate of CO_2, O_2, light energy, and nitrate could significantly affect the lipid production rate [57-60].

Sensitivity analysis of all metabolites in the metabolic network of the microalgae could be utilized for enzyme manipulation, so that the metabolism favors the production of biomass and any desirable products such as lipid, carbohydrate, protein, and chlorophyll. A positive logarithmic sensitivity represents that any increase in an input flux and decrease in an output flux of the associated metabolite can improve the optimal solution. Conversely, a negative logarithmic sensitivity shows that any decrease in influx and increase in efflux of a metabolite can enhance the optimal objective function. For instance, for a positive logarithmic sensitivity any increase in the enzymatic activity of the input fluxes and any decrease in the enzymatic activity of the output fluxes will improve the objective function. Moreover, the quality of biodiesel (physical and chemical properties of biodiesel) produced by transesterification reaction highly depends on biodiesel FAMEs composition [61, 62]. Thus, an appropriate objective function that includes the desirable fatty acids composition may be considered and optimized. Then, it would be possible to modify the enzyme activities of the key metabolites with significant sensitivities to produce high quality biodiesel with required specifications.

4. Conclusions

A flux-based approach was used to analyze a fully compartmentalized metabolic network including 347 enzymatic reactions, 195 transport processes, and 258 intracellular metabolites that were distributed among four cell compartments (chloroplast, mitochondrion, peroxisome, and cytosol) for *C. vulgaris* AG10032. The developed model was able to predict the specific growth rates with maximum relative errors of 11.74% and 13.67%, respectively, during the autotrophic cultivations without additional N-feeding and with repeated N-feeding (stage I). This model demonstrated that the microalgal cells can produce maximal lipid yield for production of biodiesel under N- starvation conditions. Metabolic flux distribution indicated that acetyl-CoA, as the main precursor for synthesis of fatty acids at TAG biosynthesis pathways, was generated by the cytosolic pyruvate upon maximization of specific growth rate and by the cytosolic citrate under maximal lipid production rate.

The model predictions also confirmed the experimental observations that a small amount of essential nutrients such as nitrate, as well as moderate levels of aeration, light intensity, and carbon dioxide can enhance the lipid content of microalgae. The highest lipid content of 43.6% was predicted by the model during N- starvation cultivation when

the following experimental conditions were applied as the model input: 100 μmol.m^{-2}.s^{-1} light intensity, 0.25 vvm aeration with 2% (v/v) CO_2, 2 mg.L^{-1} PO_4-P, and 5 mg.L^{-1} NO_3-N (stage II).

Ultimately the sensitivity analysis revealed that carbon dioxide, light energy, oxygen, and nitrate had significant effects on the algal lipid biosynthesis during the autotrophic cultivation under N-starvation.

Therefore, the proposed model provided a practical framework, by which it would be possible to predict flux distribution throughout the metabolic network of the microalgal cells and investigate the effect of nutrients and environmental conditions on the cells behavior.

Acknowledgment

This research project was funded by Ferdowsi university of Mashhad's research center (grant number 25902). The authors especially appreciate Dr. Abrishamchi for her fruitful suggestion and assistance.

Declarations

No conflicts, informed consent, human or animal rights applicable.

References

[1] G. Huang, F. Chen, D. Wei, X. Zhang, G. Chen, Biodiesel production by microalgal biotechnology,.Appl. Energ. 87 (2010) 38-46.

[2] W.L. Yu, W. Ansari, N.G. Schoepp, M.J. Hannon, S.P. Mayfield, M.D. Burkart, Modifications of the metabolic pathways of lipid and triacylglycerol production in microalgae, Microb. Cell Fact. 10 (2011) 91.

[3] Y. Li, M. Horsman, N. Wu, C.Q. Lan, N. Dubois-Calero, Biofuels from microalgae, Biotechnol. Prog. 24 (2008) 815-820.

[4] T. Minowa, S.Y. Yokoya, M. Kishimoto, T. Okakura, Oil production from algae cells of *Dunaliella Tereiolata* by direct thermochemical liquefaction, Fuel 74 (1995) 1731-1738.

[5] T.A. Milne, R.J. Evans, N. Nagle, Catalytic conversion of microalgae and vegetable oils to premium gasoline, with shape-selective zeolites, Biomass 21 (1990) 219-232.

[6] Y. Dote, S. Sawayama, S. Inoue, T. Minowa, S.-y. Yokoyama, Recovery of liquid fuel from hydrocarbon-rich microalgae by thermochemical liquefaction, Fuel 73 (1994) 1855-1857.

[7] Y. Chisti, Biodiesel from microalgae, Biotechnol. Adv. 25 (2007) 294-306.

[8] A.E.F. Abomohra, M. El-Sheekh, D. Hanelt, Screening of marine microalgae isolated from the hypersaline Bardawil lagoon for biodiesel feedstock, Renew. Energy 101 (2017) 1266-1272.

[9] C.G. Lee, B.Ø. Palsson, High-density algal photobioreactors using light-emitting diodes, Biotechnol. Bioeng. 44 (1994) 1161-1167.

[10] R.K. Mandalam, B.Ø. Palsson, Elemental balancing of biomass and medium composition enhances growth capacity in high-density *Chlorella vulgaris* cultures, Biotechnol. Bioeng. 59 (1998) 605-611.

[11] J.B. Szaub, Genetic engineering of green microalgae for the production of biofuel and high value products, Ph.D. Thesis, University College London, London, 2012.

[12] D. Surendhiran, M. Vijay, B. Sivaprakash, A. Sirajunnisa, Kinetic modeling of microalgal growth and lipid synthesis for biodiesel production, 3 Biotech. 5 (2015) 663–669.

[13] M.R. Antoniewicz, Methods and advances in metabolic flux analysis: a mini-review, J. Ind. Microbiol. Biotechnol. 42 (2015) 317-325.

[14] H. Alper, Y.S. Jin, J.F. Moxley, G. Stephanopoulos, Identifying gene targets for the metabolic engineering of lycopene biosynthesis in *Escherichia coli*, Metab. Eng. **7** (2005) 155–164.

[15] M.A. Oberhardt, J. Puchalka, K.E. Fryer, V.A.P. Martins dos Santos, J.A. Papin, Genomescale metabolic network analysis of the opportunistic pathogen *Pseudomonas aeruginosa* PAO1, J. Bacteriol. 190 (2008) 2790–2803.

[16] N.C. Duarte, M.J. Herrgard, B.Ø. Palsson, Reconstruction and validation of *Saccharomyces cerevisiae* iND750, a fully compartmentalized genome-scale metabolic model, Genome Res. 14 (2004) 1298–1309.

[17] N. Jamshidi, B.Ø. Palsson, Investigating the metabolic capabilities of *Mycobacterium tuberculosis* H37Rv using the *in silico* strain *iNJ*661 and proposing alternative drug targets, BMC Syst. Biol. 1 (2007) 26-45.

[18] M.W. Covert, E.M. Knight, J.L. Reed, M.J. Herrgard, B.Ø. Palsson, Integrating high-throughput and computational data elucidates bacterial networks, Nature 429 (2004) 92–96.

[19] J.C. Ogbonna, H. Yada, H. Tanaka, Kinetic study on light-limited batch cultivation of photosynthetic cells, J. Ferment. Bioeng. 80 (1995) 259-264.

[20] W. Van Gulik, H. Ten Hoopen, J. Heijnen, Kinetics and stoichiometry of growth of plant cell cultures of *Catharanthus roseus* and *Nicotiana tabacum* in batch and continuous fermentors, Biotechnol. Bioeng. 40 (1992) 863-874.

[21] C. Yang, Q. Hua, K. Shimizu, Energetics and carbon metabolism during growth of microalgal cells under photoautotrophic, mixotrophic and cyclic light-autotrophic/dark-heterotrophic conditions, Biochem. Eng. J. 6 (2000) 87-102.

[22] N.R. Boyle, J.A. Morgan, Flux balance analysis of primary metabolism in *Chlamydomonas reinhardtii*, BMC Syst. Biol. 3 (2009) 4-17.

[23] A. Manichaikul, L. Ghamsari, E.F. Hom, C. Lin, R.R. Murray, R.L. Chang, S. Balaji, T. Hao, Y. Shen, A.K. Chavali, Metabolic network analysis integrated with transcript verification for sequenced genomes, Nat. Methods. 6 (2009) 589-592.

[24] A.M. Kliphuis, A.J. Klok, D.E. Martens, P.P. Lamers, M. Janssen, R.H. Wijffels, Metabolic modeling of *Chlamydomonas reinhardtii*: energy requirements for photoautotrophic growth and maintenance, J. Appl. Phycol. 24 (2012) 253-266.

[25] M. Muthuraj, B. Palabhanvi, S. Misra, V. Kumar, K. Sivalingavasu, D. Das, Flux balance analysis of *Chlorella* sp. FC2 IITG under photoautotrophic and heterotrophic growth conditions, Photosynth. Res. 118 (2013) 167–179.

[26] C. Zuñiga, C.T. Li, T. Huelsman, J. Levering, D.C. Zielinski, B.O. McConnell, C.P. Long, E.P. Knoshaug, M.T. Guarnieri, M.R. Antoniewicz, M.J. Betenbaugh, K. Zengler, Genome-scale metabolic model for the green alga *Chlorella vulgaris* UTEX 395 accurately predicts phenotypes under autotrophic, heterotrophic, and mixotrophic growth conditions, Plant Physiol. 172 (2016) 589–602.

[27] E.O. Voit, Computational analysis of biochemical systems: a practical guide for biochemists and molecular biologists, first ed., Cambridge University Press, 2000.

[28] T.C. Meng, S. Somani, P. Dhar, Modeling and simulation of biological systems with stochasticity, In silico biol. 4 (2004) 293-309.

[29] R. Gheshlaghi, J. Scharer, M. Moo-Young, P. Douglas, Metabolic flux analysis for optimizing the specific growth rate of recombinant *Aspergillus niger*, Bioproc. Biosyst. Eng. 30 (2007) 397-418.

[30] C. Zupke, G. Stephanopoulos, Intracellular flux analysis in hybridomas using mass balances and in vitro ^{13}C NMR, Biotechnol. Bioeng. 45 (1995) 292-303.

[31] R. Schuetz, L. Kuepfer, U. Sauer, Systematic evaluation of objective functions for predicting intracellular fluxes in *Escherichia coli*, Mol. Syst. Biol. 3 (2007) 119.

[32] C. Wittmann, Analysis and engineering of metabolic pathway fluxes in *Corynebacterium glutamicum*, Adv. Biochem. Eng/Biotech. 120 (2010) 21-49.

[33] M.T. Guarnieri, J. Levering, C.A. Henard, J.L. Boore, M.J. Betenbaugh, K. Zengler, E.P. Knoshaug, Genome sequence of the oleaginous green alga, *Chlorella vulgaris* UTEX 395, Front. Bioeng. Biotechnol. 6 (2018) 1-2.

[34] H.W. Heldt, Plant biochemistry, third ed., Burlington, MA: Elsevier Academic Press, 2005.

[35] J.M. Berg, J.L. Tymoczko, L. Stryer, Biochemistry, fifth ed., New York: WH Freeman, 2002.

[36] L. Taiz, E. Zeiger, Plant Physiology, fifth ed., Sinauer Associates, Sunderland, MA, 2010.

[37] O. Perez-Garcia, F.M. Escalante, L.E. de-Bashan, Y. Bashan, Heterotrophic cultures of microalgae: metabolism and potential products, Water Res. 45 (2011) 11-36.

[38] M. Kanehisa, S. Goto, KEGG: kyoto encyclopedia of genes and genomes, Nucleic Acids Res. 28 (2000) 27-30.

[39] A.M.J. Kliphuis, Modeling of microalgal metabolism, Ph.D. Thesis, Wageningen University, Wageningen, 2010.

[40] M. Avron, Photosynthetic electron transport and photophosphorylation, The biochemistry of plants, 8 (1981) 163-191.

[41] C.H. Foyer, A.J. Bloom, G. Queval, G. Noctor, Photorespiratory metabolism: genes, mutants, energetics, and redox signaling, Annu. Rev. Plant Biol. 60 (2009) 455-484.

[42] L.P. de Gucht, L.H. van der Plas, Growth kinetics of glucose-limited *petunia hybrida* cells in chemostat cultures: Determination of experimental values for growth and maintenance parameters, Biotechnol. Bioeng. 47 (1995) 42-52.

[43] D.J. Murphy, Plant lipids: biology, utilisation and manipulation, John Wiley & Sons, 2009.

[44] E.P. Kennedy, Biosynthesis of complex lipids, Federation Proceedings 20 (1961) 934-940.

[45] Y. Sasaki, T. Konishi, Y. Nagano, The compartmentation of acetyl-coenzyme A carboxylase in plants, Plant Physiol. 108 (1995) 445-449.

[46] J. Ohlrogge, J. Browse, Lipid biosynthesis, The Plant Cell **7** (1995) 957-970.

[47] C. Ratledge, S. Wilkinson, An overview of microbial lipids, Microbial lipids 1 (1988) 3-22.

[48] Q. Hu, M. Sommerfeld, E. Jarvis, M. Ghirardi, M. Posewitz, M. Seibert, A. Darzins, Microalgal triacylglycerols as feedstocks for biofuel production: perspectives and advances, The Plant J. 54 (2008) 621-639.

[49] B. Wood, Fatty acids and saponifiable lipids, Algal Physiol. Biochem. 10 (1974) 236-265.

[50] D.J. Pannell, Introduction to practical linear programming, John Wiley & Sons, Inc. USA, 1997.

[51] A. Varma, B.Ø. Palsson, Metabolic capabilities of *Escherichia coli* II. Optimal growth patterns, J. Theor. Biol. 165 (1993a) 503-522.

[52] N.V. Torres, E.O. Voit, Pathway analysis and optimization in metabolic engineering, Cambridge University Press, 2002.

[53] G. Mujtaba, W. Choi, C.G. Lee, K. Lee, Lipid production by *Chlorella vulgaris* after a shift from nutrient-rich to nitrogen starvation conditions, Bioresour. Technol. 123 (2012) 279-283.

[54] D.E. Santiago, H.F. Jin, K. Lee, The influence of ferrous-complexed EDTA as a solubilization agent and its auto-regeneration on the removal of nitric oxide gas through the culture of green alga *Scenedesmus* sp., Process Biochem. 45 (2010) 1949-1953.

[55] R. Rippka, J. Deruelles, J.B. Waterbury, M. Herdman, R.Y. Stanier, Generic assignments, strain histories and properties of pure cultures of cyanobacteria, J. Gen. Microbiol. 111 (1979) 1-61.

[56] A. Illman, A. Scragg, S. Shales, Increase in Chlorella strains calorific values when grown in low nitrogen medium, Enzyme Microb. Tech. 27 (2000) 631-635.

[57] A.L. Gonçalves, J.C.M. Pires, M. Simões, Lipid production of *Chlorella vulgaris* and *Pseudokirchneriella subcapitata*, Int. J. Energy Environ. Eng. 4 (2013) 1.

[58] H. Zheng, Z. Gao, F. Yin, X. Jiand, H. Huang, Effect of CO_2 supply conditions on lipid production of *Chlorella vulgaris* from enzymatic hydrolysates of lipid-extracted microalgal biomass residues, Bioresour. Technol. 126 (2012) 24.

[59] M.J. Griffiths, R.P. van Hille, S.T.L. Harrison, The effect of nitrogen limitation on lipid productivity and cell composition in *Chlorella vulgaris*, Appl. Microbiol. Biotechnol. 98 (2014) 2345.

[60] Y.A.M. Yusof, J.M.H. Basari, N.A. Mukti, R. Sabuddin, A.R. Muda, S. Sulaiman, S. Makpol, W.Z.W. Ngah, Fatty acids composition of microalgae *Chlorella vulgaris* can be modulated by varying carbon dioxide concentration in outdoor culture, Afr. J. Biotechnol. 10 (2011) 13536.

[61] M.A. Islam, M. Magnusson, R.J. Brown, G.A. Ayoko, Md.N. Nabi, K. Heimann, Microalgal species selection for biodiesel production based on fuel properties derived from fatty acid profiles, Energies 6 (2013) 5676-5702.

[62] S.H. Al-lwayzy, T. Yusaf, R.A. Al-Juboori, Biofuels from the fresh water microalgae *Chlorella vulgaris* (FWM-CV) for diesel engines, Energies 7 (2014) 1829-1851.

Figure captions

Fig. 1. A simplified overview of key metabolic pathways in microalgae cells used for flux balance analysis. The abbreviations and corresponding reactions are given in the Appendix. The solid and dashed arrows represent enzymatic reactions and transport processes, respectively.

Fig. 2. Metabolic pathways of the biosynthesis of triglycerides in microalgae.

Fig. 3. Simulation results of metabolites production rate (in $mmol.h^{-1}$), chlorophyll (■) protein (▩) carbohydrate (□) and lipid (▨) at different phases of photoautotrophic cultivation (stage I). a, b) cultivation without N-feeding; c, d) cultivation with N-feeding.

Fig. 4. Changes in key metabolic pathways and fluxes distribution in microalgae cells during incubation under nitrogen-depleted conditions (stage II) and darkness with different aeration rates of (a) 0.125 to 0.25 vvm; (b) 0.25 to 0.5 vvm. Enzymatic reactions (solid arrows) and transport processes (dashed arrows). Increased fluxes (plus), decreased fluxes (minus), and key flux changes (numbers).

Fig. 5. Changes in key metabolic pathways and fluxes distribution in microalgae cells during incubation under N-deficient conditions (stage II) with 0.25 vvm aeration and 10 mg/L PO_4-P at different light intensities of 0 to 100 $\mu mol.m^{-2}.s^{-1}$. Enzymatic reactions (solid arrows) and transport processes (dashed arrows). Increased fluxes (plus), decreased fluxes (minus), and key flux changes (numbers).

Fig. 6. Changes in key metabolic pathways and fluxes distribution in microalgae cells during incubation with 0.25 vvm, 100 $\mu mol.m^{-2}.s^{-1}$ light intensity, 2 mg/L PO_4-P, and 5 mg/L NO_3-N under different CO_2 concentrations of (a) 0 to 2%; (b) 2 to 10%. Enzymatic reactions (solid arrows) and transport processes (dashed arrows). Increased fluxes (plus), decreased fluxes (minus), and key flux changes (numbers).

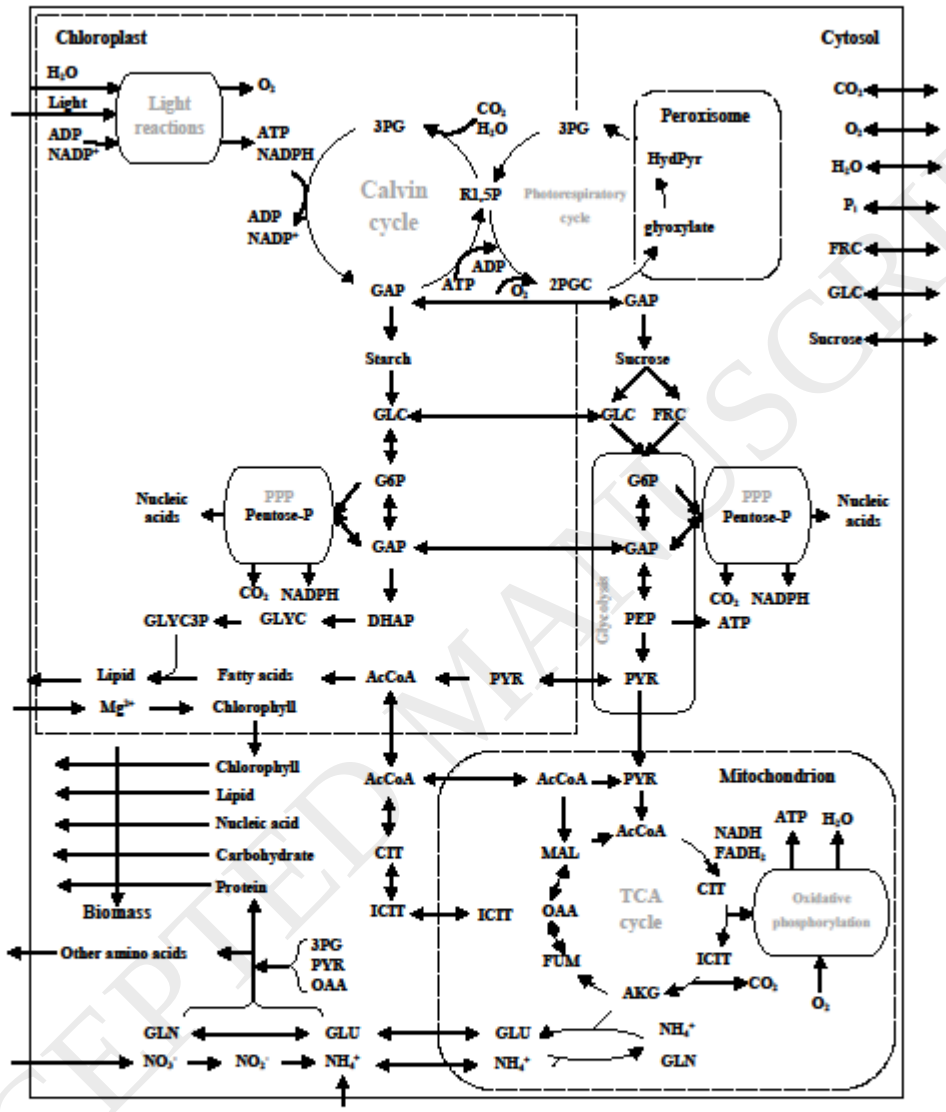

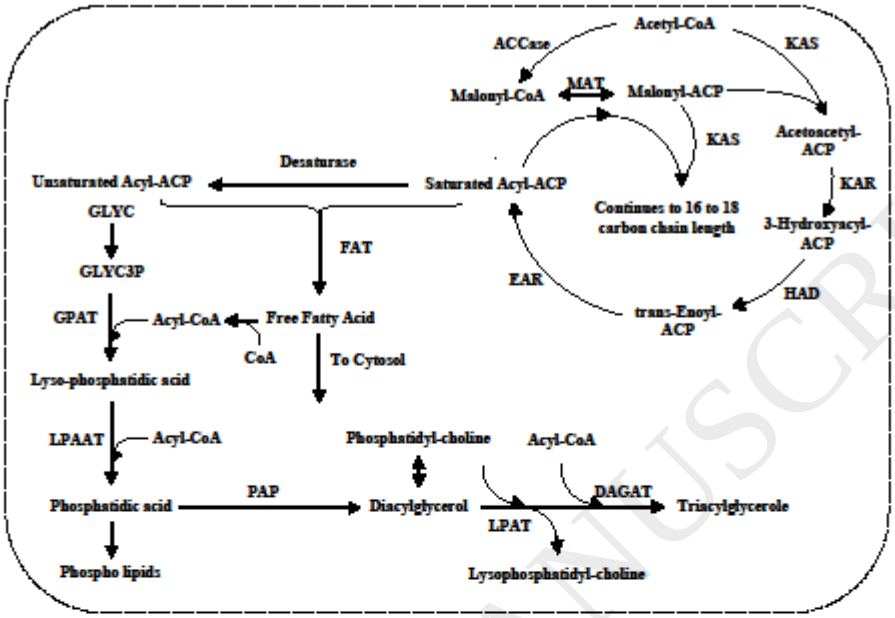

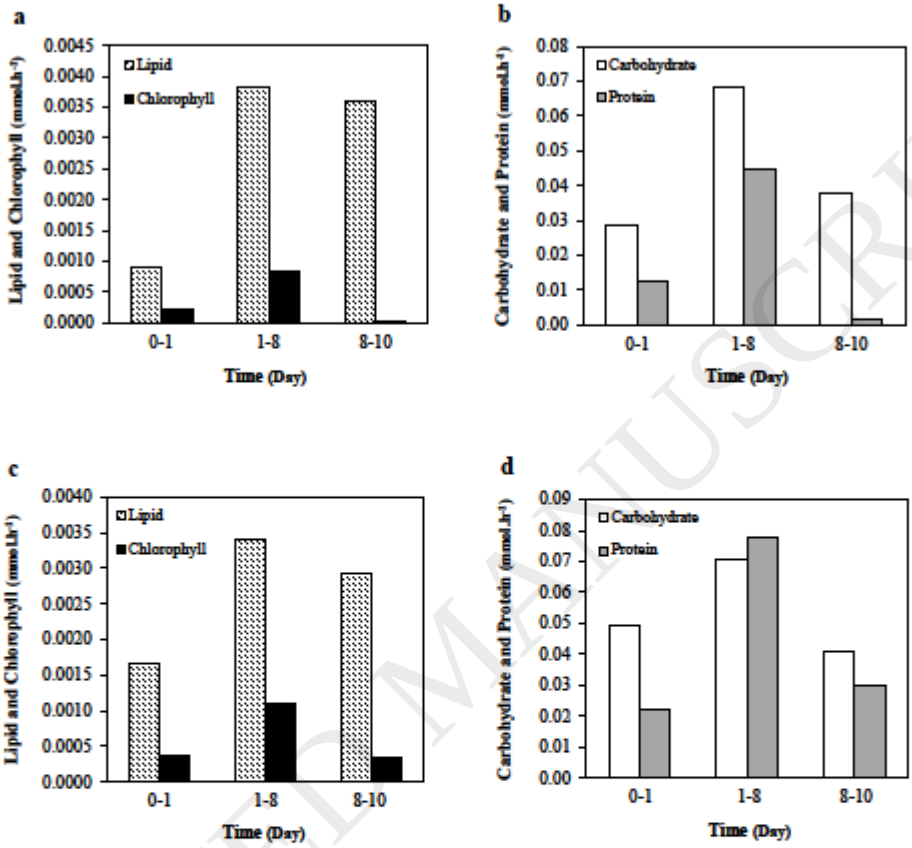

1

a

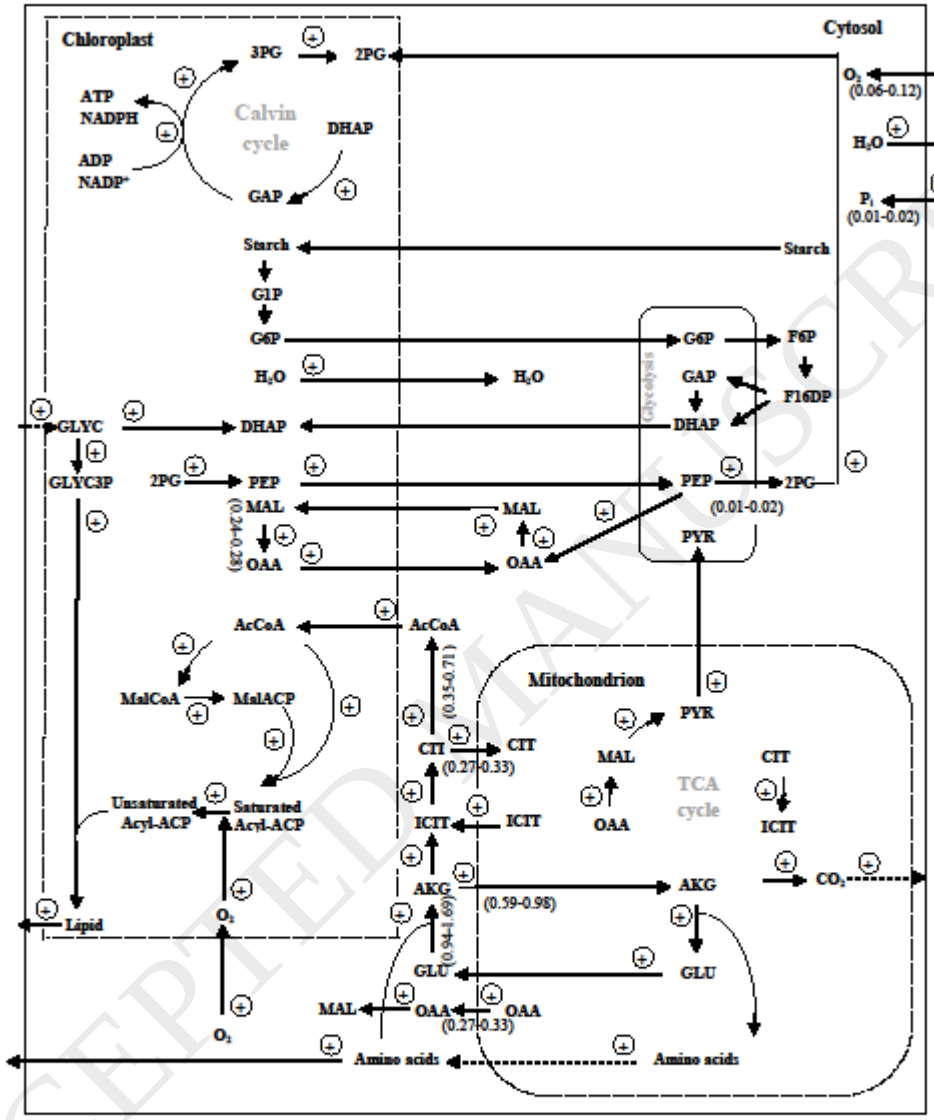

b

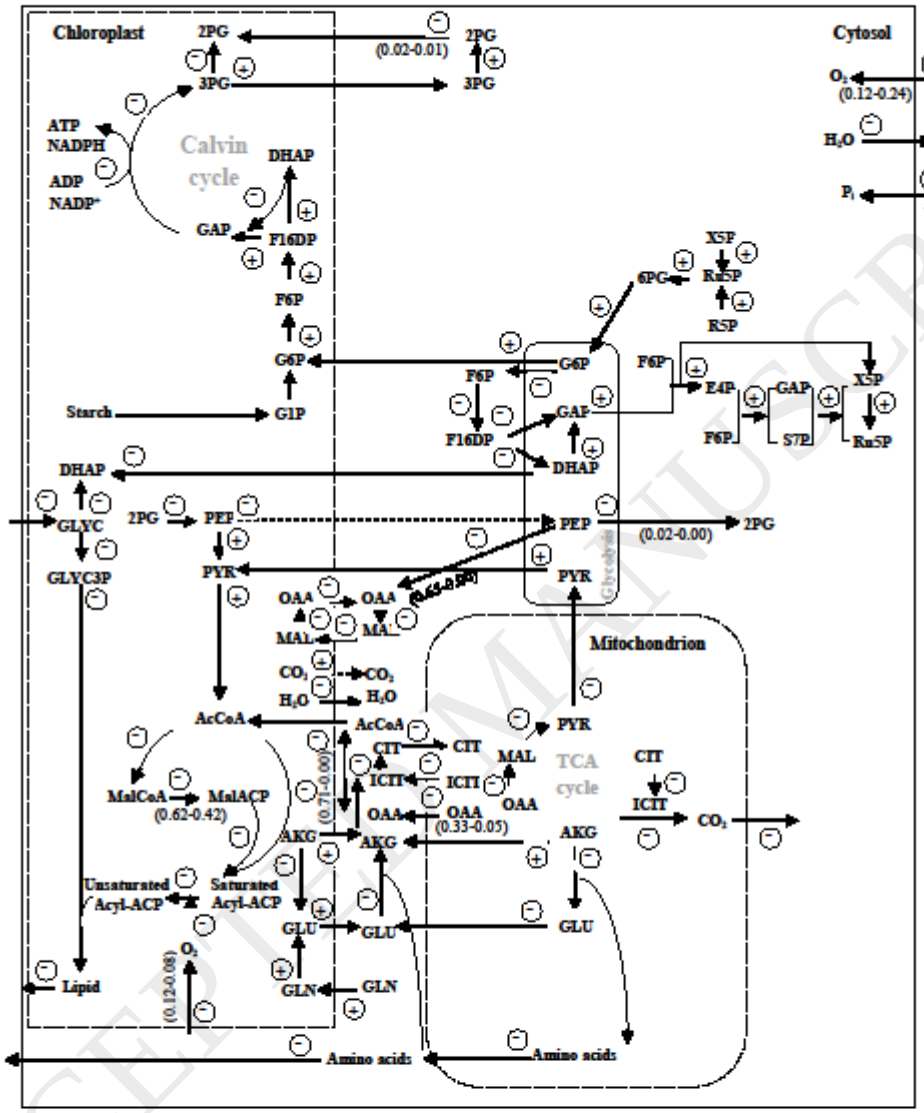

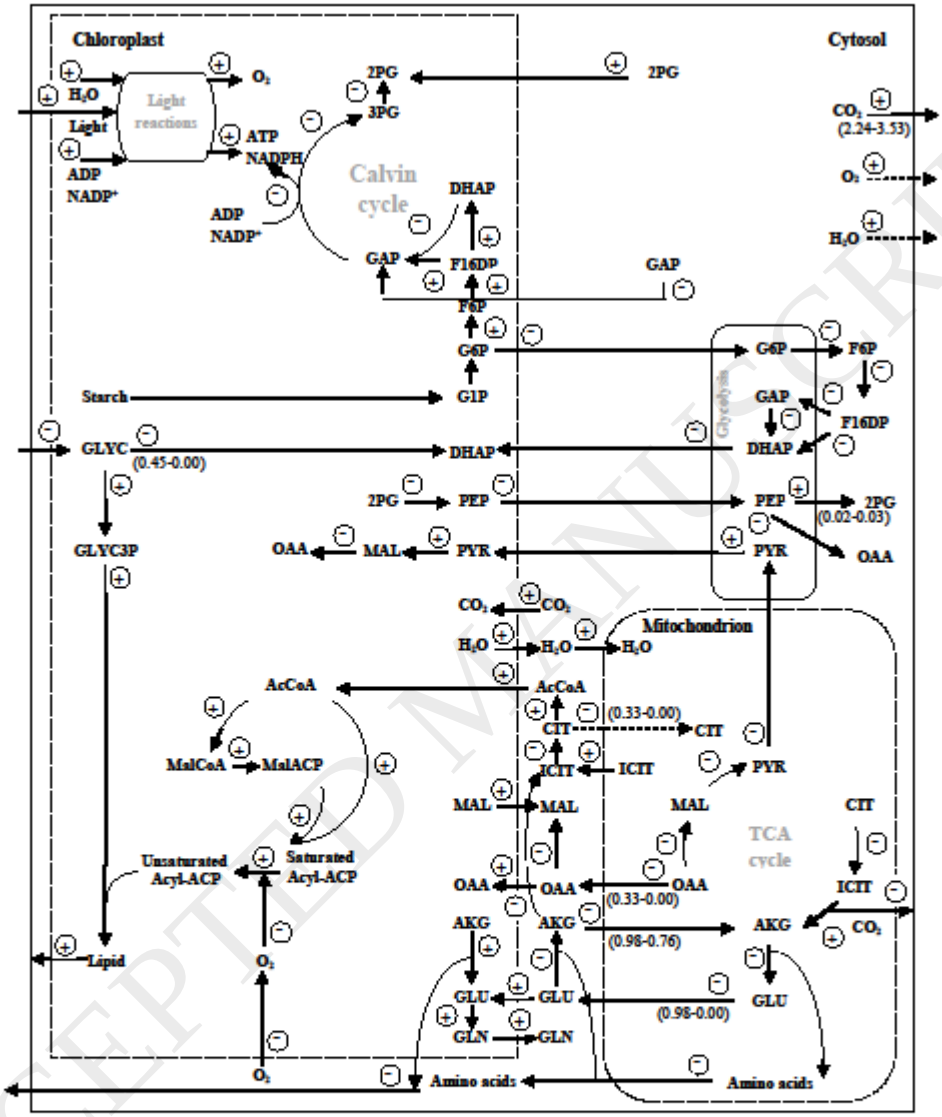

1

a

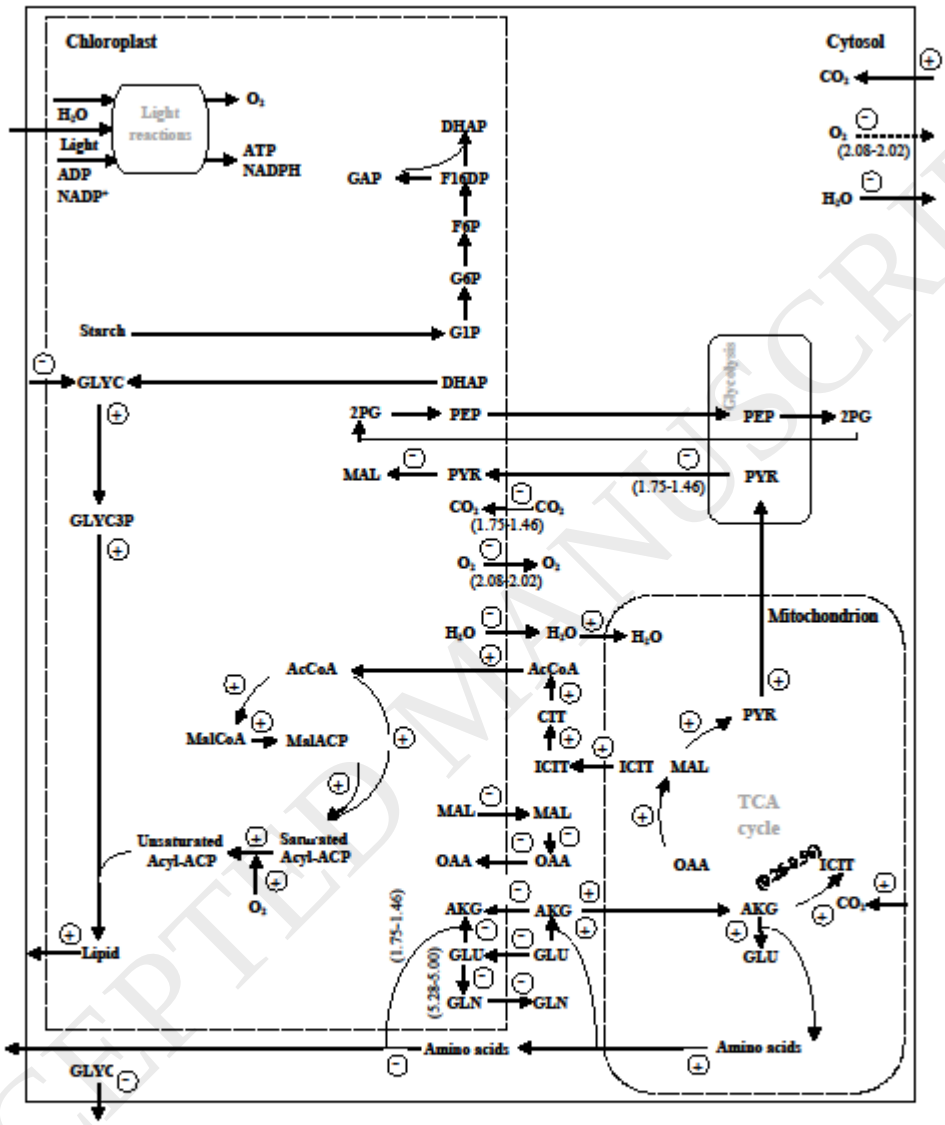

b

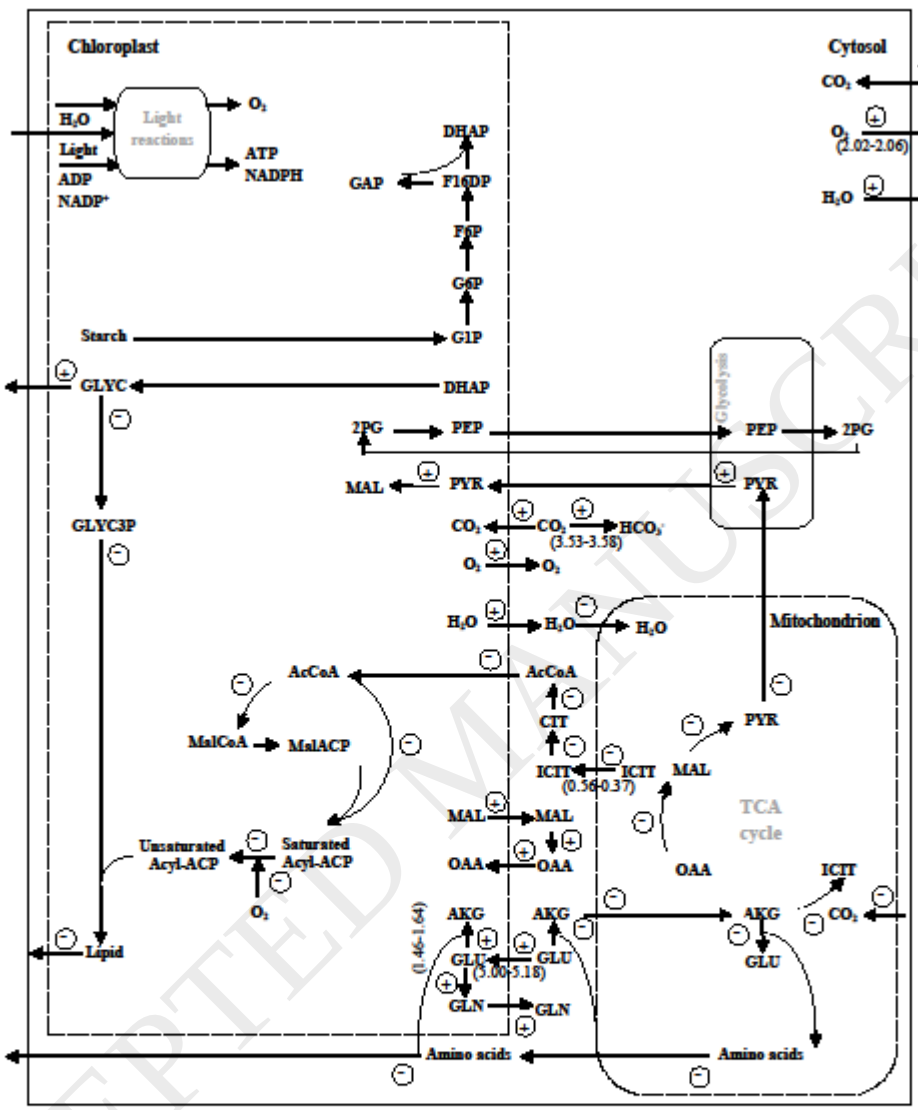

Table 1 Simulation results of specific growth rate (h^{-1}), lipid content ($mmol.g^{-1}$), LUR, CUR and OPR ($mmol.h^{-1}$) at different phases of cultivation without additional N-feeding and with repeated N-feeding (stage I) for optimum specific growth rate.

Cultivation condition	**Time (Day)**	**Model input**		**Simulation**						**Experiment[a]**			**$\lvert\%Error_{\mu}$**
		NUR[a] ($mmol.h^{-1}$)		**LUR ($mmol.h^{-1}$)**	**CUR ($mmol.h^{-1}$)**	**OPR ($mmol.h^{-1}$)**	**LC ($mmol.g^{-1}$)**	**μ (h^{-1})**		**LC ($mmol.g^{-1}$)**	**μ (h^{-1})**		
Without N-feeding	0-1	0.179		4.347	0.186	0.538	0.043	0.09308		0.036	0.08330		11.74
	1-8	0.076		10.870	0.455	1.344	0.425	0.00997		0.165	0.00931		7.09
	8-10	0.005		6.522	0.220	0.815	0.553	0.00029		0.235	0.00027		7.41
With N-feeding	0-1	0.181		4.386	0.297	0.539	0.054	0.09469		0.036	0.08330		13.67
	1-8	0.106		10.870	0.576	1.339	0.203	0.01050		0.143	0.00983		6.82
	8-10	0.011		6.525	0.284	0.807	0.247	0.00273		0.157	0.00250		9.20

[a] The experimental data represent the mean ± SD for n =3 (Fig. 1(a) of [53]).

Table 2 Simulation results of lipid content (mmol.g^{-1}), LUR, CUR and OPR (mmol.h^{-1}) at different phases of cultivation without N-feeding and with N-feeding (stage I) for optimum lipid production rate.

Cultivation condition	**Time (Day)**	**Model input**			**Simulation**					**Experiment[a]**
		NUR[a] (mmol.h^{-1})	**μ[a] (h^{-1})**		**LUR (mmol.h^{-1})**	**CUR (mmol.h^{-1})**	**OPR (mmol.h^{-1})**	**LC (mmol.g^{-1})**		**LC (mmol.g^{-1})**
Without N-feeding	0-1	0.179	0.08330		4.347	0.295	0.526	1.523		0.036
	1-8	0.076	0.00931		10.870	0.735	1.304	3.201		0.165
	8-10	0.005	0.00027		6.522	0.442	0.797	3.324		0.235
With N-feeding	0-1	0.181	0.08330		4.386	0.297	0.519	1.485		0.036
	1-8	0.106	0.00983		10.870	0.736	1.305	2.723		0.143
	8-10	0.011	0.00250		6.525	0.441	0.793	2.794		0.157

[a] The experimental data represent the mean ± SD for n =3 (Fig. 1(a) of [53]).

Table 3 Effects of cultivation factors on lipid contents of *C. vulgaris* under different conditions of the cultivation (stage II).

Factors	Cultivation condition					Lipid content (%)		$\lvert\%\ Error_{LC}\rvert$
	Aeration rate (vvm)	Light intensity ($\mu mol.m^{-2}.s^{-1}$)	PO_4-P ($mg.L^{-1}$)	NO_3-N ($mg.L^{-1}$)	CO_2 (%)	Experiment[a]	Simulation	
Aeration rate	0.125	0	-	0	0	26.8	27.2	1.49
	0.250	0	-	0	0	28.5	34.1	19.65
	0.500	0	-	0	0	23.4	29.5	26.07
Light intensity	0.250	0	10	0	0	28.0	34.1	21.79
	0.250	100	10	0	0	32.7	35.1	7.34
	0.250	200	10	0	0	30.6	35.5	16.01
CO_2 supply	0.250	100	2	5	0	37.4	32.2	13.90
	0.250	100	2	5	2	43.0	43.6	1.40
	0.250	100	2	5	10	32.8	36.1	10.06

[a] The experimental data represent the mean ± SD for n =3 (Fig. 2, 3, and 6 of [53]).

Table 4 Shadow prices and logarithmic sensitivities for various metabolites at different phases of autotrophic cultivation without N-feeding (stage I) for maximum lipid production.

Metabolites	λ_i **(dimensionless)**				$\lvert L(Z,V_i)\rvert$ **(dimensionless)**		
	0-1 Day	**1-8 Day**	**8-10 Day**		**0-1 Day**	**1-8 Day**	**8-10 Day**
CO_2	0.000	0.525	0.450		0.000	39.711	57.731
O_2	0.000	-0.019	-0.021		0.000	2.549	4.866
Photon	0.000	0.024	0.000		0.000	26.844	0.000
P_i	0.015	0.026	0.025		0.004	0.011	0.023
NO_3	0.000	-0.130	-0.270		0.000	1.019	3.87
NH_4	0.000	-0.350	-0.485		0.000	0.000	0.000
GLYC	0.025	0.545	0.648		0.000	0.000	0.000
PRO	0.003	0.000	0.000		0.069	0.000	0.000
PHE	0.001	0.001	0.000		0.001	0.000	0.000
Sucrose	0.000	-0.014	0.000		0.000	0.000	0.000
RNA	0.000	0.002	0.000		0.000	0.000	0.000
DNA	0.000	0.000	0.000		0.000	0.000	0.000
Protein	0.000	0.034	0.000		0.000	0.000	0.000
Chlorophyll	0.000	0.000	0.000		0.000	0.000	0.000